Coherent State Evolution in a Superconducting Qubit from Partial-Collapse Measurement

N. Katz,[1] M. Ansmann,[1] Radoslaw C. Bialczak,[1] Erik Lucero,[1] R. McDermott,[1] Matthew Neeley,[1] Matthias Steffen,[1] E. M. Weig,[1] A. N. Cleland,[1] John M. Martinis,[1]* A. N. Korotkov[2]

Measurement is one of the fundamental building blocks of quantum-information processing systems. Partial measurement, where full wavefunction collapse is not the only outcome, provides a detailed test of the measurement process. We introduce quantum-state tomography in a superconducting qubit that exhibits high-fidelity single-shot measurement. For the two probabilistic outcomes of partial measurement, we find either a full collapse or a coherent yet nonunitary evolution of the state. This latter behavior explicitly confirms modern quantum-measurement theory and may prove important for error-correction algorithms in quantum computation.

The wave-particle duality in quantum mechanics originates from two distinct ways in which a quantum state may change: a linear (unitary) evolution according to the Schrödinger wave equation and a nonlinear (projective or "collapse") evolution due to measurement (*1*). In recent years, it has been understood that an interesting combination of wave and particle dynamics can be observed by using partial measurements, in which the quantum state both partially collapses and coherently evolves at the same time (*2*). In quantum optics, continuous quantum measurement back-action was harnessed to control state evolution, leading to the generation of squeezed states (*3*). Also, partial measurement is predicted to be useful as a form of quantum-error correction, in which continuous feedback is used for correction (*4*). We present full experimental verification of a partial measurement on a solid-state qubit (*5*–*9*) that is also a macroscopic quantum system (*10*, *11*). The simplicity of our partial measurement presents a clear demonstration of this phenomenon (*12*), shedding light on the physics of quantum measurements.

Recent experiments (*13*–*16*) with superconducting circuits, fabricated using lithographic techniques, have provided an intriguing link between microscopic quantum states and macroscopic quantum phenomena. Many important coherent effects, familiar from quantum optics and nuclear magnetic resonance explorations, have been reproduced in such devices. Energy relaxation and dephasing of these Josephson qubits have also been extensively studied (*6*, *7*, *17*, *18*), leading to the development of various techniques to further enhance the lifetime of the qubit state. However, the delicate issue of measurement (*19*) and the subsequent evolution of the qubit have received less attention (*16*, *20*–*23*). Substantial progress has been made to overcome low measurement visibilities (*16*, *20*, *21*, *23*), measurement back-action (*17*, *20*), short lifetimes of superposition states (*5*, *16*, *23*), and difficulties in integrating complex pulse sequences with arbitrary phase and amplitude. Many of these problems are now resolved in the Josephson phase qubit. By using our recent improvements in rapid measurements (*16*, *22*), quantum state tomography (*23*, *24*), and measurement fidelity, we can now explicitly demonstrate the coherent aspects of nonunitary state evolution during a partial measurement. This further places the phase qubit as a major candidate for scalable quantum-information processing in the solid state.

In a schematic of the phase qubit (*16*, *25*) circuit (Fig. 1A), the superconducting phase difference across the Josephson junction (with critical current I_0) is δ, which serves as our quantum variable. A control flux bias is introduced into the inductor L, and the total current $I_\phi = I_{dc} + I_z(t)$ [where I_{dc} is a constant current and $I_z(t)$ is a time (t)–dependent current pulse] biases the junction and adjusts the cubic potential (Fig. 1, B and C). This, in turn, determines the height of the energy-potential barrier ΔU and the transition frequency $\omega_{10}/2\pi$. The qubit state is coherently manipulated by on-resonant microwave-frequency (μw) pulses $I_{\mu w}$ (in the 5- to 10-GHz range) that drive transitions between the basis states. Smooth control pulses I_z on the bias line (generated from room temperature voltage pulses V_z and a cold μw bias tee) are used to vary the frequency difference ω_{10} adiabatically,

[1]Department of Physics and California NanoSystems Institute, University of California, Santa Barbara, CA 93106, USA. [2]Department of Electrical Engineering, University of California, Riverside, CA 92521, USA.

*To whom correspondence should be addressed. E-mail: martinis@physics.ucsb.edu

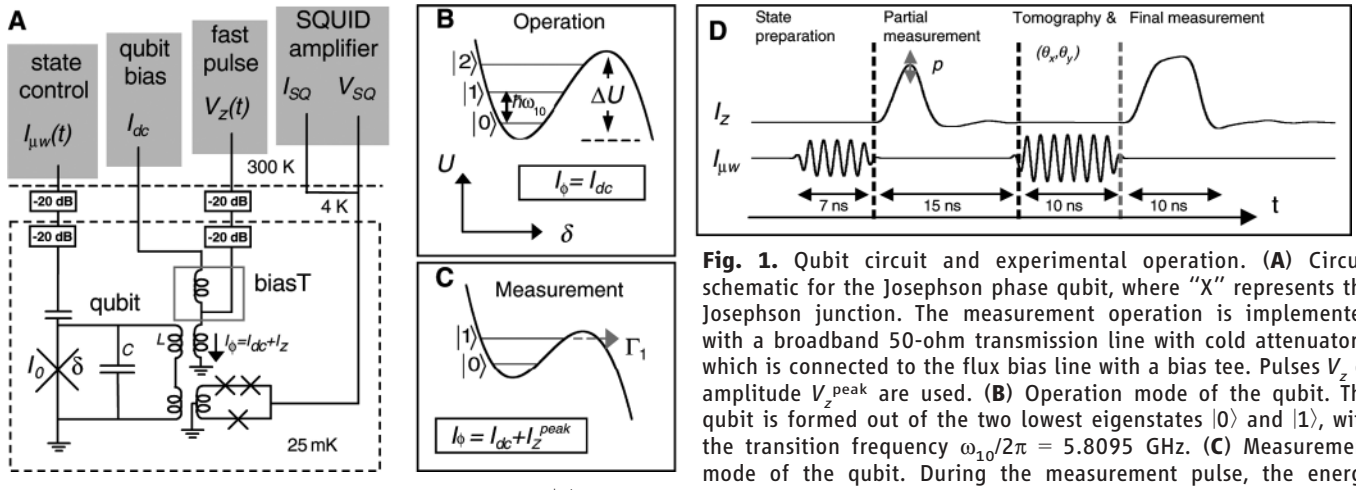

Fig. 1. Qubit circuit and experimental operation. (**A**) Circuit schematic for the Josephson phase qubit, where "X" represents the Josephson junction. The measurement operation is implemented with a broadband 50-ohm transmission line with cold attenuators, which is connected to the flux bias line with a bias tee. Pulses V_z of amplitude V_z^{peak} are used. (**B**) Operation mode of the qubit. The qubit is formed out of the two lowest eigenstates $|0\rangle$ and $|1\rangle$, with the transition frequency $\omega_{10}/2\pi = 5.8095$ GHz. (**C**) Measurement mode of the qubit. During the measurement pulse, the energy barrier ΔU is lowered so that the tunneling probability of $|1\rangle$ increases. (**D**) Timing of the experiment. The microwave sequence $I_{\mu w}(t)$ includes the initial preparatory pulse and the later tomographic pulse. The bias current $I_\phi(t)$ is held at the constant value I_{dc} during the microwave pulses and is pulsed to higher values $I_{dc} + I_z(t)$ for the partial and full measurements. The experimental bias current is shown, including a ~3% ringing after the pulses.

leading to the accumulation of a controlled phase between the $|0\rangle$ and $|1\rangle$ states. When the bias current is pulsed to higher values $I_{dc} + I_z^{peak}$ (Fig. 1C), the rate of tunneling Γ_1 of the $|1\rangle$ state out of the metastable qubit potential becomes large. Tunneling is a selective measurement of the $|1\rangle$ state because the rate from the $|0\rangle$ state is typically slower by a factor of about 200. Furthermore, Γ_1 is exponentially sensitive to ΔU, and we may vary the amplitude of the measurement pulse I_z^{peak} to tunnel a controlled fraction p of the $|1\rangle$ state population out of the well. Once tunneled, the state decays rapidly to an external ground state. The coherence with the wavefunction component remaining in the qubit well is lost in less than 0.3 ns (*25*) and constitutes the partial collapse. The two components are distinguished at a later time by the on-chip superconducting quantum interference device (SQUID) amplifier and readout circuitry.

The timeline of the experimental sequence is shown in Fig. 1D. We first apply a microwave pulse (typically 7 ns in duration) to prepare the qubit in a known state. This is followed by a short (3.2-ns full-width at half maximum) partial-measurement pulse. The remaining qubit state is then analyzed by a second tomographic microwave pulse (10 ns in duration) followed by a final full-measurement ($p \cong 1$) pulse. For a given initial state and partial measurement, the complete tomographic determination of a state involves scanning over all phases and a range of amplitudes of the tomographic pulse (Fig. 2). For each pixel in the two-dimensional scan of tomography pulses, data are taken 200 times to acquire sufficient statistics to determine the resulting qubit populations.

Ideally, the initial qubit state prepared by the first microwave pulse can be described as a superposition $|\psi_0\rangle = \cos(\theta_0/2)|0\rangle + e^{-i\phi_0}\sin(\theta_0/2)|1\rangle$, where θ_0 and ϕ_0 are polar and azimuthal angles on the Bloch sphere (*12*) in the rotating frame. This pulse is used to define the initial phase $\phi_0 = 0$.

A partial measurement leads to a nontrivial evolution of the quantum state (*2*, *12*), with the net probability for each eventuality on the right,

$$|\psi_0\rangle \rightarrow \begin{cases} |\psi_M\rangle = \frac{1}{N}[\cos(\theta_0/2)|0\rangle + e^{-i\phi_M}\sqrt{1-p} \times \sin(\theta_0/2)|1\rangle] & 1 - p\sin^2(\theta_0/2) \\ \text{tunnel out of qubit well} & p\sin^2(\theta_0/2) \end{cases} \quad (1)$$

where $N = [\cos^2(\theta_0/2) + (1 - p)\sin^2(\theta_0/2)]^{1/2}$ is the normalization and ϕ_M is an acquired phase (M indicates measured). Casting $|\psi_M\rangle$ into a normalized form $|\psi_M\rangle = \cos(\theta_M/2)|0\rangle + e^{-i\phi_M}\sin(\theta_M/2)|1\rangle$, we find

$$\theta_M = 2\tan^{-1}\left[\sqrt{1-p}\tan(\theta_0/2)\right] \quad (2)$$

For the subset of events that do not tunnel from the partial measurement, the change from θ_0 to θ_M constitutes the coherent and nonunitary evolution of the qubit state due to partial measurement. As p approaches unity, the state is fully projected into the state $|0\rangle$, as expected. Notably, because of the normalization factor, the amplitude of the state $|0\rangle$ increases even though this state is not explicitly

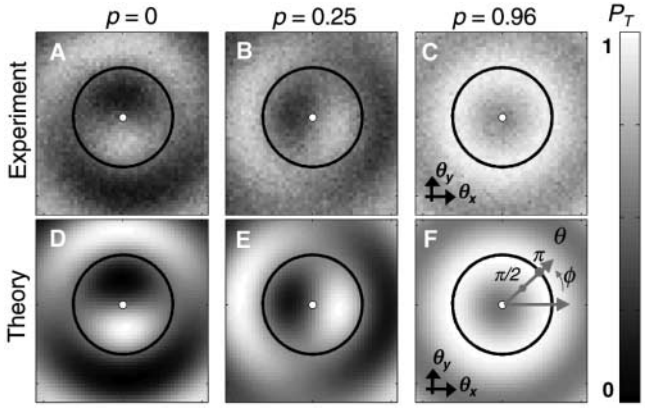

Fig. 2. Tomographic scan of the qubit state, initially at $\theta_0/\pi = 0.53\ (\pm 0.02)$, following partial measurements. The central spots mark $\theta = 0$ and the circles correspond to $\theta = \pi$. (**A** to **C**) Experimental tomographic probabilities P_T for $p = 0$, 0.25, and 0.96. We observe a clear change in P_T from an antisymmetric ($p = 0$) to a nearly symmetric ($p = 0.96$) distribution. (**D** to **F**) Fitted distributions for the data of (A) to (C). The distributions are in marked agreement, given the simplicity of the model. The primary difference is the reduced visibility of the experimental data, which is quantified in Fig. 3C.

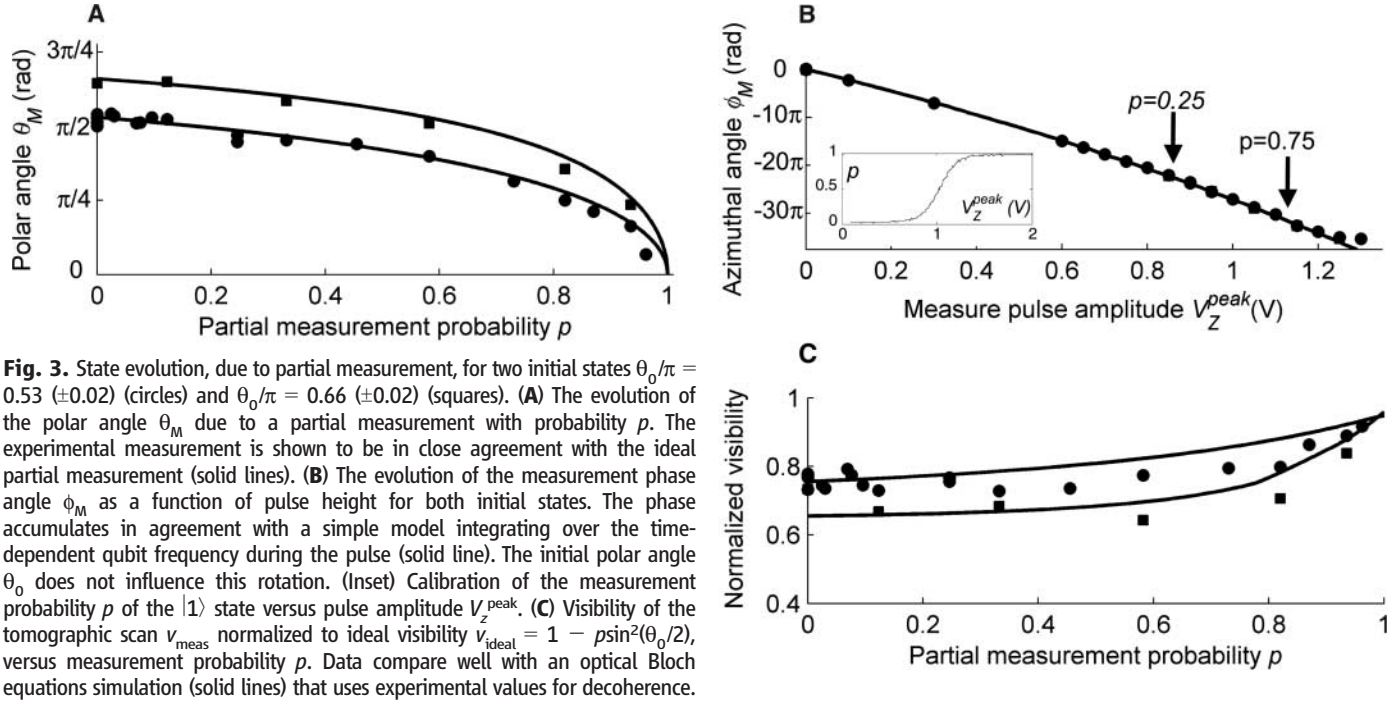

Fig. 3. State evolution, due to partial measurement, for two initial states $\theta_0/\pi = 0.53\ (\pm 0.02)$ (circles) and $\theta_0/\pi = 0.66\ (\pm 0.02)$ (squares). (**A**) The evolution of the polar angle θ_M due to a partial measurement with probability p. The experimental measurement is shown to be in close agreement with the ideal partial measurement (solid lines). (**B**) The evolution of the measurement phase angle ϕ_M as a function of pulse height for both initial states. The phase accumulates in agreement with a simple model integrating over the time-dependent qubit frequency during the pulse (solid line). The initial polar angle θ_0 does not influence this rotation. (Inset) Calibration of the measurement probability p of the $|1\rangle$ state versus pulse amplitude V_z^{peak}. (**C**) Visibility of the tomographic scan v_{meas} normalized to ideal visibility $v_{ideal} = 1 - p\sin^2(\theta_0/2)$, versus measurement probability p. Data compare well with an optical Bloch equations simulation (solid lines) that uses experimental values for decoherence.

measured. Because these events did not undergo any tunneling or subsequent decay, the accumulated phase ϕ_M can be calculated (in this simple model) from the frequency dependence on the time-varying bias current and is given by $\int_0^{T_p}[\omega_{10}(I_\phi(t)) - \omega_{10}(I_{dc})]dt$, for a pulse of duration T_p.

The resulting state $|\psi_M\rangle$ is determined with the tomographic microwave pulse, which only changes $|\psi_M\rangle$ and does not influence the tunneled population outside the qubit well. The tomography pulse, with components θ_x and θ_y in the *xy* plane of the Bloch sphere, rotates the qubit state by an angle $\theta = \sqrt{\{\theta_x^2 + \theta_y^2\}}$ around the direction $\phi = \tan^{-1}(\theta_y/\theta_x)$ (Fig. 2F). The resulting state is therefore given by

$$|\psi_T\rangle = \left[\cos(\theta_M/2)\cos(\theta/2) - \sin(\theta_M/2)\sin(\theta/2)e^{i(\phi-\phi_M)}\right]|0\rangle + \left[\cos(\theta_M/2)\sin(\theta/2) + \sin(\theta_M/2)\cos(\theta/2)e^{i(\phi-\phi_M)}\right]|1\rangle \quad (3)$$

The final measurement pulse causes tunneling of the $|1\rangle$ state component of $|\psi_T\rangle$ (T indicates tomography). This results in the total measured probability of tunneling

$$P_T = p\sin^2(\theta_0/2) + [1 - p\sin^2(\theta_0/2)]\left|\langle 1|\psi_T\rangle\right|^2 = 1 - \frac{1 - p\sin^2(\theta_0/2)}{2} \times \left[1 + \cos(\theta_M)\cos(\theta) - \sin(\theta_M)\sin(\theta)\cos(\phi - \phi_M)\right] \quad (4)$$

which includes the original $p\sin^2(\theta_0/2)$ probability from the partial-measurement pulse summed with the additional probability from the final measurement.

The measured distributions of P_T are shown in Fig. 2, A to C, as a function of the tomographic parameters (*26*). We saw a change in the symmetry of the distributions from an antisymmetric pattern (Fig. 2A) to a symmetric one (Fig. 2C), demonstrating the evolution of the qubit state due to the partial measurement, as θ_M changes continuously from the initial state value of $\sim\pi/2$ to ~ 0. In addition to the change in θ_M, we observed a rapid and repeatable rotation of the distribution of P_T due to the expected coherent accumulation of phase ϕ_M (Fig. 2B). Theoretical fits to P_T are used to determine θ_M and ϕ_M, with p, θ_0, ϕ_0, θ, and ϕ calibrated separately. Fitted distributions, displayed in Fig. 2, D to F, capture the main features of the data.

In the plots of θ_M and ϕ_M versus probability p and pulse amplitude V_z^{peak} (Fig. 3, A and B), the measurements were carried out for two different initial states (±SD) $\theta_0/\pi = 0.53$ (±0.02) and $\theta_0/\pi = 0.66$ (±0.02). We observed convincing agreement between Eq. 2 and experiment with no fit parameters, indicating the validity of the nonunitary description of the partial measurement operator in Eq. 1. The agreement (*25*) of the measured ϕ_M with the expected phase calculated from $\omega_{10}(I_\phi)$ indicates that rapid pulsing of the flux bias can also be used as a high-fidelity z-gate.

This idealized picture of state evolution is not fully realized in our experiment because of energy relaxation and dephasing. Ideally, the measured probabilities in Fig. 2 should oscillate between $p\sin^2(\theta_0/2)$ and unity, leading to a visibility $v_{ideal} = 1 - p\sin^2(\theta_0/2)$ in P_T. In practice, the experimental visibility is less. Figure 3C shows the measured visibility v_{meas} of the experiment divided by v_{ideal}. We calculated the expected visibility by solving the optical Bloch equations (*12*) with the use of the experimental parameters of energy relaxation time (T_1 = 110 ns) and dephasing time (T_2 = 80 ns) obtained in a separate experiment. In the calculation, the measurement is taken to be an instantaneous change of the Bloch vector according to the generalized quantum description of the partial measurement operator acting on a density matrix state (*12*). The good agreement between experiment and simulation, with no fit parameters, shows that the partial measurement is indeed applying a rapid evolution of the state, in full agreement with Eq. 1, with very little added decoherence (less than 4%). The slight asymmetries in the experimental patterns, barely visible on Fig. 2, A to C, are traced to the effect of the off-resonant state $|2\rangle$ (Fig. 1B), with a population that is measured to never exceed 2% during the entire experiment. Further enhancements in qubit lifetimes and careful shaping of the microwave pulses will allow us to reduce this unwanted occupation even further.

Measurement is a critical component of fault-tolerant quantum computation as it is widely used in quantum error–correction algorithms (*27*). Instantaneous measurement of a qubit state is typically used to project the remaining encoded qubits to the correct state, improving the fidelity of the calculation. This experiment shows in detail that the evolution of the quantum state with measurement is obeying the quantum mechanical predictions. In any realistic, experimental implementation, slow and incoherent measurements will rapidly degrade the success of error correction by adding uncontrolled decoherence. Our measurement scheme is thus attractive because it is both fast and coherent.

Rapid pulsing of the bias for a phase qubit has been shown to be a well-defined quantum operator of partial measurement and high-fidelity z-rotation. The speed, visibility, and coherence of this measurement technique are expected to be well suited for determining multiple qubit states, including violation of Bell inequalities for two qubit states, and for use in quantum error–correction codes.

References and Notes

1. M. Schlosshauer, *Rev. Mod. Phys.* **76**, 1267 (2004).
2. J. Dalibard, Y. Castin, K. Mølmer, *Phys. Rev. Lett.* **68**, 580 (1992).
3. J. M. Geremia, J. K. Stockton, H. Mabuchi, *Science* **304**, 270 (2004).
4. C. Ahn, H. M. Wiseman, G. J. Milburn, *Phys. Rev. A.* **67**, 052310 (2003).
5. Y. Nakamura, Y. A. Pashkin, J. S. Tsai, *Nature* **398**, 786 (1999).
6. D. Vion *et al.*, *Science* **296**, 886 (2002).
7. J. M. Martinis, S. Nam, J. Aumentado, C. Urbina, *Phys. Rev. Lett.* **89**, 117901 (2002).
8. I. Chiorescu, Y. Nakamura, C. J. P. M. Harmans, J. Mooij, *Science* **299**, 1869 (2003).
9. J. Q. You, F. Nori, *Phys. Today* **58**, 42 (2005).
10. J. M. Martinis, M. H. Devoret, J. Clarke, *Phys. Rev. Lett.* **55**, 1543 (1985).
11. J. R. Friedman, V. Patel, W. Chen, S. K. Tolpygo, J. E. Lukens, *Nature* **406**, 43 (2000).
12. M. A. Nielsen, I. L. Chuang, *Quantum Computation and Quantum Information* (Cambridge Univ. Press, Cambridge, 2000).
13. A. Wallraff *et al.*, *Nature* **431**, 162 (2004).
14. I. Chiorescu *et al.*, *Nature* **431**, 159 (2004).
15. W. D. Oliver *et al.*, *Science* **310**, 1653 (2005).
16. K. B. Cooper *et al.*, *Phys. Rev. Lett.* **93**, 180401 (2004).
17. P. Bertet *et al.*, *Phys. Rev. Lett.* **95**, 257002 (2005).
18. J. M. Martinis *et al.*, *Phys. Rev. Lett.* **95**, 210503 (2005).
19. A. N. Korotkov, *Phys. Rev. B* **63**, 115403 (2001).
20. A. Wallraff *et al.*, *Phys. Rev. Lett.* **95**, 060501 (2005).
21. A. Lupascu, E. F. C. Driessen, L. Roschier, C. J. P. M. Harmans, J. E. Mooij, *Phys. Rev. Lett.* **96**, 127003 (2006).
22. R. McDermott *et al.*, *Science* **307**, 1299 (2005).
23. M. Steffen *et al.*, *Cond. Mater.*, in press; preprint (http://arxiv.org/abs/cond-mat/0602432).
24. G. M. D'Ariano, M. G. A. Paris, M. F. Sacchi, *Adv. Imaging Electron Phys.* **128**, 205 (2003).
25. Materials and methods are available as supporting material on *Science* Online.
26. The quantum-state tomography shown here can be implemented in different ways. Typically, only three high-precision measurements are needed for a single qubit. For multiple qubit–state tomography, of course, such a simplified scheme becomes mandatory. However, the full two-dimensional scan allows us to resolve the rotation angle with high precision, determine the visibility shown in Fig. 3C, easily avoid any calibration errors in the microwave frequency, and fully test for proper state rotations.
27. P. W. Shor, *Phys. Rev. A.* **52**, R2493 (1995).

28. We acknowledge S. Waltman and the National Institute for Standards and Technology for support in building the microwave electronics. Devices were made at the University of California at Santa Barbara and Cornell Nanofabrication Facilities, a part of the NSF-funded National Nanotechnology Infrastructure Network. N.K. acknowledges support of the Rothschild fellowship. This work was supported by Advanced Research and Development Activity under grant W911NF-04-1-0204 and NSF under grant CCF-0507227.

Supporting Online Material

www.sciencemag.org/cgi/content/full/312/5779/1498/DC1
Materials and Methods
Fig. S1

21 February 2006; accepted 20 April 2006
10.1126/science.1126475